UNEC Journal of Engineering and Applied Sciences
Vol. 6, No.1, 2026, pp. 26-38
DOI: https://doi.org/10.61640/ujeas.2026.0503

SECTION: ENGINEERING SCIENCES

Sea lion optimization algorithm-based proportional-derivative neural-network controller for nonlinear suspension system design

H. Al-Khazraji*, M. Nawfal, R.A. Kadhim, M.M. Msallam, O.F. Lutfy

University of Technology- Iraq, Al-Wehda Neighborhood, Baghdad 10066, Iraq
email: *60141@uotechnology.edu.iq*

Abstract

This study develops a proportional-derivative neural-network (PD-NN) controller for active suspension systems represented by nonlinear dynamics and actuator saturation. To ensure optimal performance, the sea lion optimization (SLO) has been employed to improve the search process for the optimal values of the weights in the neural network. Computer simulations are carried out to compare the new PD-NN controller with the conventional PD controller. The simulation results of the comparative study illustrate that the PD-NN controller has the best handling and comfort performance for active suspension systems. Furthermore, the simulation results using MATLAB based on minimizing the Integral Square Error (ISE) index show that the proposed controller exhibits good performance for both normal operation and operation with uncertainty in the system parameters compared to the standalone PD controller.

***Keywords*:** active suspension systems, nonlinear dynamics, proportional-derivative controller, neural-network, actuator saturation, sea lion optimization.

PACS numbers: 07.05.Dz, 87.55.de, 82.20.Wt

Received:	*Revised:*	*Accepted:*	*Published:*
2 September 2025	*12 December 2025*	*18 February 2026*	*31 May 2026*

1. Introduction

One of the most significant necessities of modern life has become people's use of vehicles for long periods and over vast distances, which necessitates that car be more comfortable and safer in numerous aspects. These include maintaining the appropriate temperature and humidity inside the vehicle throughout the year, sound insulation, noise reduction, and maintaining clean air inside the vehicle's cabin. Furthermore, other requirements include lighting, window design, seat quality and comfort, ensuring sufficient space for passengers, and, more recently, even psychological factors for enjoyment, such as screens and some entertaining electronic games [1-4]. All of these requirements are important factors to provide comfort for passengers while riding in the vehicle. However, other factors directly influence the health and safety of the driver and passengers, namely the vibration level and the car suspension system. In particular, the driver is continuously exposed to vibration at a constant rate, which will increase the driver's likelihood of drowsiness and the potential risk of joint and spinal pain [5-6]. Consequently, researchers and engineers have focused extensively and have devoted considerable attention to giving the suspension system great importance in design, adjustment, and improvement to achieve the utmost comfort and safety together, as evidenced by numerous studies published in reputable scientific journals and presented at leading international conferences, all aiming to provide both comfort and safety. To handle this difficulty, evident and well-known physical concepts build the

conventional (passive) automobile suspension system, which is still applied until now in numerous good car's brands because it has sundry characteristics that encourage vehicle manufacturers to adopt it as a simple, cheap, safe, reliable, easy to install, clear and easy to maintain system. However, it is considered unable to react to road bump variables in a way that better serves the comfort of passengers and drivers [7-8].

In order to enhance the performance limitations of passive suspension systems, researchers proposed the development of semi-active suspension systems. These systems included an advanced type of dampers with an adjustable damping coefficient that enables improving ride comfort and vehicle stability and energy efficiency, while maintaining manageable structural and design complexity [9-11]. However, despite all the wonderful advantages offered by semi-active suspension systems, there are certain applications and utilizations that demand the use of active suspension systems. These systems provide superior ride comfort, highly precise control, adaptive response capabilities, and consistent performance across a wide range of road conditions. For instance, luxury sedans require maximum comfort and adaptive suspension behavior to deliver a premium driving experience. On the other hand, sports cars and supercars demand exceptional handling, minimal body roll, and stability at high speeds. In autonomous vehicles, suspension systems must ensure platform stability for sensor accuracy and passenger comfort. Meanwhile, heavy-duty trucks and armored vehicles require active load leveling and consistent stability under varying payloads and operational conditions [12-13]. The foundation of all the above-mentioned suspension systems lies in the conventional vibration model that comprises a mass, a spring, and a shock absorber. This basic setup has long been used to manage how vehicles respond to bumps and road irregularities. In semi-active suspension systems, the key innovation lies in the damper whose damping coefficient can be adjusted in real-time, allowing the system to adapt to varying driving conditions and improve ride quality. Active suspension systems take the concept even further. In addition to an adaptive damper, they include an actuator that actively generates cancelling forces to equalize road disturbances, which allows for precise control, offering enhanced comfort, stability, and adaptability across a wide range of driving conditions [14-16]. In this paper, a mathematical model of an active suspension system is presented that includes all the nonlinear parameters of the system, which necessitates the use of robust controllers to achieve the desired design goal.

In this context, the works in [17-19] confirmed that the performance of feedback control systems is satisfactory and ensures the stability, accuracy, and efficiency of the systems. The researchers continually presented their work in this field with impressive and practical designs, which inspired us to develop a controller capable of enhancing comfort for travellers. For instance, Shahid and Wei [20] investigated the active vibration control of a quarter-vehicle suspension system using various control methods, including higher-order sliding mode control (HOSMC) based on the super twisting algorithm, the first-order sliding mode control (FOSMC), the integral sliding mode control (ISMC), the proportional integral derivative (PID), the linear quadratic regulator (LQR), and the passive suspension. The performance of these controllers was compared based on vertical displacement, suspension movement, and wheel deflection. The results showed that the HOSMC with the super twisting algorithm surpasses other methods by providing better vibration suppression and robustness against model uncertainties and external disturbances. In another work, an innovative approach involving a full-vehicle active suspension controller (ASC) with a low-order controller was presented in [21], aiming to improve passenger comfort and reduce suspension movement. This approach integrates the sliding Mode Control (SMC) system with the Fuzzy Logic Control (FLC) system through the fuzzy sliding-mode control (FSMC) system. More specifically, the SMC system focuses on reducing suspension displacement, while the FLC system addresses ride quality. Comparative simulations considering the optimal active suspension control (OASC) scheme across multiple road conditions have shown that the fuzzy sliding-mode control (FSMC) system achieves better suspension comfort and control

compared to other conventional methods. In addition, Dai et al. [22] improved the performance of an active suspension system by designing a nonlinear active disturbance rejection control (NLADRC) system for the suspension system of a two-degree-of-freedom (2DFR) quarter-truck model, with the aim of improving system performance under dynamic disturbances. The proposed control system was compared with conventional control strategies, including proportional-integral-differential (PID) control and linear active disturbance rejection control. Moreover, Zhang et al. [23] focused on improving both ride comfort and vehicle height regulation in nonlinear active air suspension systems. To address the inherent uncertainties, conventional controllers struggle to balance these objectives. Therefore, an adaptive control algorithm was proposed. In this regard, the findings in [24] highlighted that the PID controller has superior performance and robustness under system uncertainties in comparison with the state feedback controller. In particular, the grey wolf optimization (GWO) was introduced to improve the searching process for the optimal values of the controllers' adjustable parameters. Meanwhile, Kemer and Başak [25] focused on the development of intelligent control systems, specifically Fuzzy-LQR and Fuzzy-LQG, to enhance the performance of active suspension systems in automobiles, regardless of road input signals. These control strategies were evaluated through MATLAB/Simulink simulations and benchmarked against conventional passive suspension systems as well as standard LQR and LQG controllers. The results demonstrated that the intelligent controllers significantly improved ride comfort by reducing the vertical acceleration of the vehicle body, with RMS values decreasing by up to 74.25% in certain scenarios.

While prior research has led to notable improvement for the active suspension systems, the exploration and investigation of new control strategies continue to be an active area of investigation. In this direction, this study proposes an integration of proportional-derivative with a feed-forward neural network (PD-NN) for enhancing the dynamic performance of active suspension systems in order to reduce or eliminate the road excitations transmitted to the vehicle body. Particularly, the nonlinearities and actuator saturation are incorporated into the mathematical model of the suspension system for a more reasonable representation of the real system. To train the weights of the PD-NN controller and to avoid the drawbacks of gradient-based optimization methods, the sea lion optimization (SLO) is employed. Moreover, the performance of the proposed controller is compared to that of the standalone PD controller.

2. Mathematical modeling

A diagram of two degrees of freedom of the active suspension system represented by the quarter car model is illustrated in figure 1 [14].

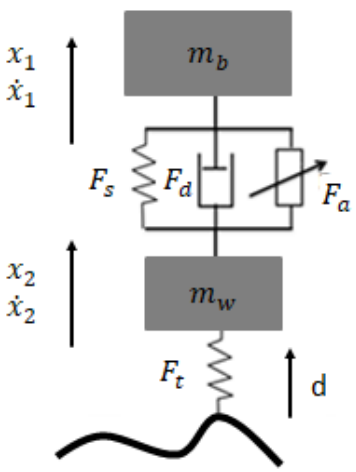

Figure 1. Active suspension system represented by a quarter car model

This model consists of the mass of a quarter of the car body (m_b) and the single wheel mass (m_w). These masses are connected using a spring and a viscous damper to represent the stiffness and damping of the shock absorber . F_s and F_d are the forces generated by the wheel spring and the wheel damper, respectively. The spring and the damper are typically connected in parallel for several important physical and engineering reasons. Specifically, the spring provides support and allows motion, while the damper controls oscillations and stabilizes the system. Each of these components shares the same displacement but handles different types of forces [7]. In the context of a linear model, the force F_S generated by the spring that stores and releases energy based on displacement is represented by:

$$F_S = -k\,x \tag{1}$$

where x and k are the position and the spring stiffness, respectively. In addition, the damper main function is to dissipate energy through resistance to velocity, and it converts the energy to heat. Therefore, the force depends on the velocity as follows:

$$F_d = -c\,\dot{x} \tag{2}$$

where $\dot{x}$ and c are the velocity and the damping coefficient, respectively. Despite the simplicity of the linear representation of the spring and the damper, linear models provide approximate results that do not fully reflect reality, especially at high speeds or large vibrations. In particular, the spring material behavior used at high loads may not follow Hook's law $F = k\,x$, and the geometric nonlinearity of the spring, such as progressive–rate springs, are designed so that their stiffness changes with displacement. In addition, the hysteresis and internal friction in a real spring can exhibit energy loss and path- dependent behavior, leading to nonlinear force responses depending on the motion history and not just position. Moreover, the mechanical constraints and physical limits like bump stops or end stops cause the spring to behave nonlinearly when those limits are reached. Additionally, in side loading and buckling that occur when the spring is subjected to lateral forces or bending, the axial force no longer increases linearly with displacement, producing nonlinear effects. Therefore, the force-displacement relationship of the spring element becomes [26]:

$$F_S = k_1\,x + k_2\,x^3 \tag{3}$$

where k_1 is the linear stiffness coefficient and k_2 is the nonlinear stiffness coefficient. In the same way, the force often follows a nonlinear relationship. This is especially common in high-speed damping situations like aerodynamic or hydraulic damping. The shock absorber is one of the most important elements in a vehicle suspension system, and it is also one of the most nonlinear and complex elements in the model. Therefore, the nonlinear damper characteristic of the suspension in real-world dampers is given by [14]:

$$F_d = c_1\,\dot{x} + c_2\dot{x}^2 \tag{4}$$

where c_1 is the linear damping coefficient and c_2 is the nonlinear damping coefficient. In order to develop the mathematical model of the nonlinear suspension system, the spring force (F_s) and the damping force (F_d) are given by:

$$F_s = k_{sl}(x_1 - x_2) + k_{sn}(x_1 - x_2)^3 \tag{5}$$

$$F_d = c_{dl}(\dot{x}_1 - \dot{x}_2) + c_{dn}(\dot{x}_1 - \dot{x}_2)^2 \tag{6}$$

where x_1 and x_2 are the positions of the body and the wheel, respectively. The parameters k_{sl}, k_{sn}, c_{dl} and c_{dn} denote to the linear and nonlinear stiffness coefficients of the spring,

followed by the linear and nonlinear damping coefficients of the damper, respectively. The equation of motion considering the vertical displacement of the car body with nonlinear suspension characteristics based on the Newten's law can be written as:

$$m_b\ddot{x}_1 = -F_s - F_d + F_a \tag{7}$$

$$m_w\ddot{x}_2 = F_s + F_d - F_a - F_t \tag{8}$$

where $\ddot{x}_1$ and $\ddot{x}_2$ are the acceleration variables of the car body and the wheel, respectively, F_a and F_t are the forces of the actuator and the spring of the tire, respectively. The force (F_t) is:

$$F_t = k_t(x_2 - d) \tag{9}$$

where d is the road disturbance and k_t is the tire's spring stiffness coefficient. By substituting equation (1) and equation (2) into equation (3) and equation (4), we obtain:

$$m_b\ddot{x}_1 = -(k_{sl}(x_1 - x_2) + k_{sn}(x_1 - x_2)^3) - (c_{dl}(\dot{x}_1 - \dot{x}_2) + c_{sn}(\dot{x}_1 - \dot{x}_2)^2) + F_a \tag{10}$$

$$m_w\ddot{x}_2 = (k_{sl}(x_1 - x_2) + k_{sn}(x_1 - x_2)^3) + (c_{dl}(\dot{x}_1 - \dot{x}_2) + c_{sn}(\dot{x}_1 - \dot{x}_2)^2) - F_a - \left(k_t(x_2 - d)\right) \tag{11}$$

Nonlinear suspension modeling is not just a mathematical enhancement, but rather it is a fundamental requirement for integrating artificial intelligence and modern control technologies. This transition enables cars to respond more intelligently and efficiently to road conditions, improving both safety and ride comfort. For the purpose of the control design, the state variable equations of the nonlinear suspension system are defined as:

$$\dot{x}_1 = x_3 \tag{12}$$

$$\dot{x}_2 = x_4 \tag{13}$$

$$\dot{x}_3 = \frac{1}{m_b}\left((-(k_{sl}(x_1 - x_2) + k_{sn}(x_1 - x_2)^3) - (c_{dl}(\dot{x}_1 - \dot{x}_2) + c_{sn}(\dot{x}_1 - \dot{x}_2)^2) + F_a)\right) \tag{14}$$

$$\dot{x}_4 = \frac{1}{m_w}\left((k_{sl}(x_1 - x_2) + k_{sn}(x_1 - x_2)^3) + (c_{dl}(\dot{x}_1 - \dot{x}_2) + c_{sn}(\dot{x}_1 - \dot{x}_2)^2) - F_a - \left(k_t(x_2 - d)\right)\right) \tag{15}$$

where $\dot{x}_3$ and $\dot{x}_4$ are the acceleration variables of the car body and the wheel, respectively.

3. Controller design

This section presents the detailed design procedure of the Proportional-Derivative Feed-Forward Neural Network (PD-NN) controller for the nonlinear suspension system. To enhance passenger comfort, the intelligent control unit was designed to eliminate the disruptive vibrations that passive suspension systems are unable to manage. To this end, neural network (NN) techniques have demonstrated strong potential for controlling nonlinear systems due to their self-learning ability, adaptability, and effectiveness in handling nonlinear dynamics [27-28]. In particular, the NN is composed of interconnected processing elements called neurons (n), which are linked to each other through adjustable parameters known as weights (w) [29–30]. One of the most important features of these weights is their ability to

learn independently in order to accurately map the relationship between the system's inputs and outputs. Over time, the performance of a neural network improves through frequently readjusting of its weights in the network. The weights of the NN can then be adjusted via the so-called backpropagation algorithm. Besides the backpropagation algorithm, many authors exploited the swarm optimization to optimize and enhance the NN performance [31-32]. The PD-NN controller block diagram is shown in figure 2.

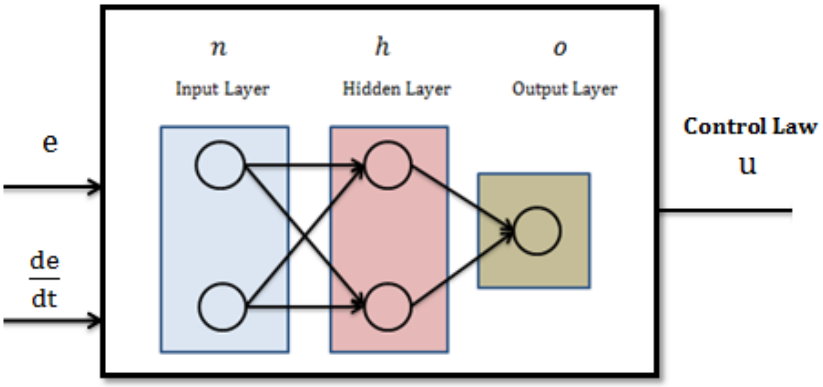

Figure 2. Structure of the PD-NN controller

The proposed PD-NN controller architecture consists of three feedforward layers: the input layer (n), the hidden layer (h), and the output layer (o). Motivated by the concept of the PD controller, two inputs are considered in the input layer, including the present error and the derivative of the error. In addition, the hidden layer contains two neurons with the tanh activation function. Lastly, the output layer o has one neuron with a linear activation function. In mathematical terms, the control law of the PD-NN controller is given by:
hidden layer (h):

$$h_j = \tanh(\sum_{i=1}^{2} w_i\, n_i)\,, j = 1,2 \tag{16}$$

output layer (o):

$$o = \sum_{j=1}^{2} w_j \;\; h_j \tag{17}$$

4. Sea lion optimization

To solve complex optimization problems, especially in high–dimensional and nonlinear search spaces, swarm optimization can be used [33-36]. In this regard, the sea lion optimization (SLO) [37] is a nature-inspired metaheuristic algorithm that mimics the social and hunting behavior of sea lions in the wild. The core concept of SLO simulates how sea lions explore the ocean in search of prey and cooperate during the hunt using spiral movements when closing in on a target (prey). The algorithm balances exploration (searching new areas) and exploitation (focusing on promising regions) to effectively converge toward optimal solutions. In the general mathematical model, the position of each sea lion is updated using mathematical formulas that involve: current position, best known position, control parameters for exploration, spiral movement equations. The most important operations of the SLO are discussed below.

4.1. The Detecting and Tracking Stage

Sea lions move uniformly and randomly in the search space, representing their search for prey. The whiskers on sea lions are one of its most distinctive characteristics producing a highly sensitive indicator of the size and position of the prey. This phase ensures diversity in

solutions and avoids premature convergence and when promising solutions are found, the sea lions start moving toward them and call others to join the group to gather around the prey in spiral paths before attacking. Such behaviors are described by the equation below [38]:

$$X_{i,j}^{init} = X_{i,j}^{min} + rand_{i,j}\,(X_{i,j}^{max} - X_{i,j}^{min}) \tag{18}$$

where $i = 1,2,\dots,N$, $j = 1,2,\dots,D$, $X_{i,j}^{init}$ is the initial position vector of the ith solution, $X_{i,j}^{min}$ and $X_{i,j}^{max}$ denote the minimum and maximum values for the jth dimension of the ith solution, respectively, and rand is a uniform random value in the interval [0, 1]. To evaluate the solution fitness, the objective function and the new position of the search agent are considered as given below [39]:

$$X^{t+1} = X_{best} - A|2rX_{best} - X^{t}| \tag{19}$$

where X_{best} and X^{t} are the position vector of the best solution and the sea lion in iteration t, respectively. The parameter A is a variable with linearly decreased values from 2 to 0 throughout the iteration, indicating the encircling mechanism of the sea lion group when they move towards the prey and surround them, as given below:

$$A = 2\left(1 - \frac{t}{T_{max}}\right) \tag{20}$$

where t and T_{max} are the current iteration and the maximum number of iterations, respectively. Equation (20) is multiplied by 2 to increase the search operation range. This parameter, A, decreases over time, shifting the focus from exploration to exploitation.

4.2. The Vocalization Stage

In the SLO algorithm, the vocalization stage is inspired by the natural behavior of the sea lions when they emit vocal sounds to communicate, attract attention, or signal others. This stage represents a local exploitation phase, where the sea lion adjusts its position based on the best-known position and certain stochastic (random) factors. A typical position update equation during the vocalization stage may look like [39]:

$$X_i^{t+1} = X_i^{t} + V\,(X_{best} - X_i^{t}) + r.\ rand \tag{21}$$

where X_i^{t} is the position of the ith sea lion solution at ilteration t, V is the vocalization factor (the strength of influence from the best position), and r is a random coefficient. The purpose of this stage is to intensify the search around the best-known position, simulate communication behavior among sea lions, and exploit promising areas of the search space. The leader lion directs the sea lion group toward what it perceives as a beneficial direction and governs their collective behavior, which can be mathematically modeled as shown in equation (22) [40].

$$SP_{leader} = |(\sin\theta\,(1 + \sin\varphi)/\sin\varphi| \tag{22}$$

where SP_{leader} is the value that illustrates the decision of the leader followed by other sea lions in the group, θ and φ are the angles of voice reflection and the voice refraction in the water, respectively.

4.3. Attacking (the Exploitation Phase)

The attacking phase is one of the key stages in the SLO algorithm. It simulates the behavior of sea lions closing in on their prey once its location is identified. When the sea lion

moves rapidly toward the best-known solution, the focus shifts from exploration to exploitation, leading to a reduction in randomness, and the movement becomes more focused and precise. The purpose of this stage is to exploit the best solution area more effectively and to allow sea lions to converge on the optimal solution quickly and efficiently. A common equation used during the attacking phase is:

$$X_i^{t+1} = X_{best}(t) + C.(X_{best}(t) - X^t) \tag{23}$$

where C is the convergence coefficient that usually decreases over time to allow fine-tuned adjustments. A new updated position of a sea lion can be located anywhere in the search space between its current position and the location of the best agent using the parameter l with a random number in the range [−1, 1]

$$X^{t+1} = X_{best} + \cos(2\pi l)\,|X_{best} - X^t| \tag{24}$$

4.4. Searching for the Prey (the Exploration Phase)

This phase is part of SLO algorithm, which is inspired by the hunting behavior of sea lions. This phase represents the early stage of the search process when sea lions are not yet aware of the prey's exact location, and hence, they search randomly in the solution space over a wide area, attempting to locate regions where the prey (the optimal solution) might be hiding. This step helps to avoid local optima by encouraging global search and balancing random movement and attraction to good positions, which causes the chances of finding the global optimum to increase before the algorithm starts fine-tuning. Finally, the exploration means that the agents try to discover new areas in the search space. The condition that allows the exploitation phase to take place is when the value of a variable with linearly decreased values from 2 to 0 throughout the iteration becomes greater than 1. The equation for finding a new agent is presented by [39]:

$$X^{t+1} = X_{rand}^t - A\left|2r\,X_{rand}^t - X^t\right| \tag{25}$$

where X_{rand}^t is a random sea lion, which is randomly selected from the current population.

5. Results and discussion

This section presents the MATLAB simulation results for the PD-NN controller used to control the nonlinear suspension system. To simulate the dynamics of the suspension system, eqs. (12–15) are used. For the purpose of comparison, the results of the PD-NN controller are compared with the results of the standalone PD controller and the results obtained in [24]. Table 1 provides the parameters of the system [24].

To simulate the road disturbance profile, eq. (26) is used to represent two bumps [24]:

$$d(t) = \begin{cases} \gamma_1(1-\cos(4\pi t_{sim})), & 0.5 \le t_{sim} \le 1 \\ \gamma_2(1-\cos(4\pi t_{sim})), & 3 \le t_{sim} \le 3.5 \\ 0, & \text{otherwise} \end{cases} \tag{26}$$

where the terms γ_1 and γ_2 define the height of the bumps, where their values are selected to be 0.02 and 0.03, respectively. For the SLO, the Integral Square Error (ISE) criterion was chosen as a cost function to train the PID-NN and the SF-NN controllers. The formula of this ISE index is [24]:

$$ISE = \int_0^{t_m} e^2\,dt \tag{27}$$

where the error between the position of the body mass x_1 and the intended trajectory is represented by the output deviation (e), and t_m stands for the simulation time.

Parameters	Value
Body mass (m_b)	500 Kg
Wheel mass (m_w)	40 Kg
Linear stiffness of the spring (k_{sl})	16021 N/m
Nonlinear stiffness of the spring (k_{sn})	180000 N/m^3
Stiffness of the tire spring (k_t)	240000 N/m
Linear damping factor of the damper (c_l)	1419 Ns/m
Nonlinear damping factor of the damper (c_n)	400 Ns^2/m^2

Table 1. System parameters

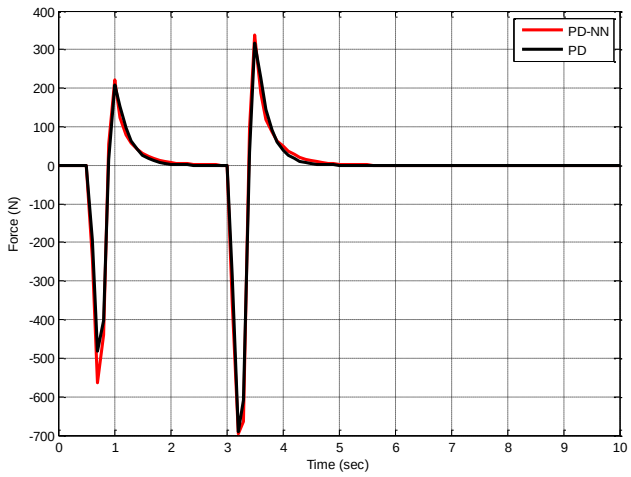

Figure 3. Control law of the controllers under normal operation

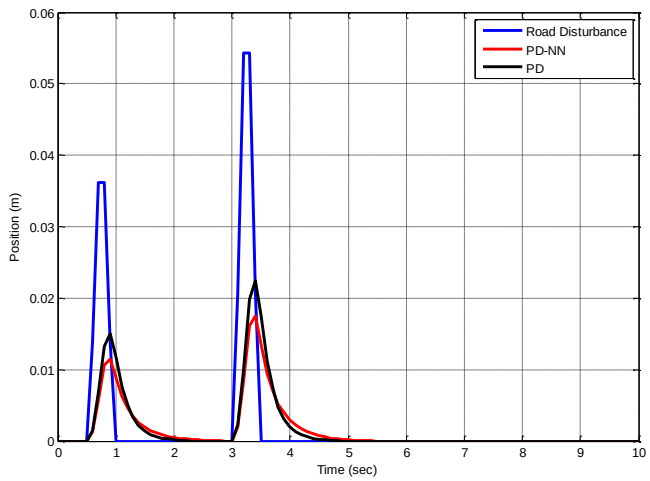

Figure 4. Suspension system response based on the PD-NN and the PD controllers

Controller	ISE
PD-NN	1.5×10^{-3}
PD	2.2×10^{-3}
PID [24]	2×10^{-3}
SF [24]	2.4×10^{-3}

Table 2. Performance comparison under normal operation

It is important to note that the actuator's input force to the suspension system is saturated by approximately 800 N. Consequently, the suspension system's controller tuning procedure based on the SLO can be expressed as an optimization problem in the following form [24]:

$$\begin{gathered}\text{minimize ISE}\\ \text{s.t}\\ -700 \leq u \leq 700\end{gathered} \tag{28}$$

where the objective function to be minimized is denoted by the letter ISE. Consequently, a constraint in the optimization problem is imposed by the saturation limit of the control input u. The control law and the responses of the two controlled systems are shown in figures 6 and 7, respectively. In addition, the numerical value of the ISE is listed in table 3. As shown in figure 6, the control signals for both controllers remain within the actuator's permissible force limit. Furthermore, figure 7 shows that the PD-NN controller outperformed the PD controller in terms of performance. The numerical validation of the result is presented in table 3, where it is apparent that the ISE index value for the PD-NN controller is (1.5×10^{-3}), which is lower than that of the ISE index value for the PD controller of (2.2×10^{-3}). However, based on table 3, it can be seen that the ISE index for the PD-NN controller is less than the ISE index of the standalone PID and SF controllers.

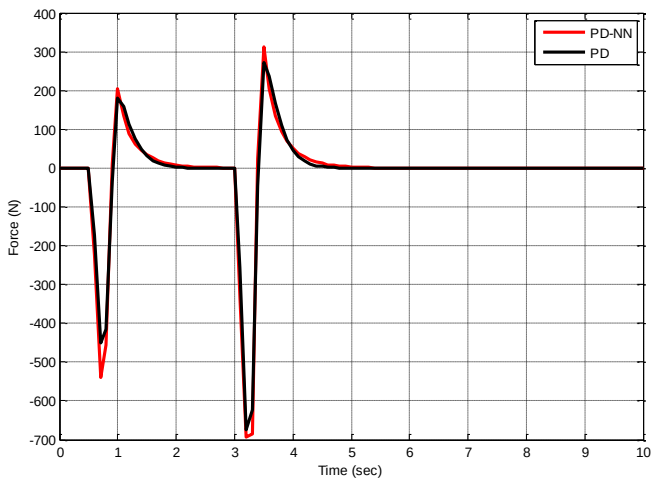

Figure 5. Control law of the controllers under a 20% increase in the car body mass

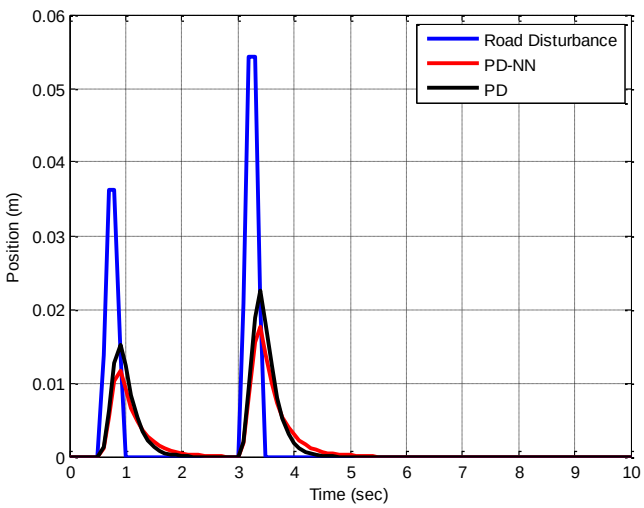

Figure 6. Suspension system response under a 20% increase in the car body mass

Controller	ISE
PD-NN	1.5×10^{-3}
PD	2.2×10^{-3}
PID [24]	2.1×10^{-3}
SF [24]	2.5×10^{-3}

Table 3. Performance comparison under 20% increase in the car body mass

The mass of the vehicle is inherently variable, as it depends on the number of occupants riding in the vehicle. Accordingly, a ±20% variation in the car body's nominal mass was assumed to evaluate the robustness of the two controllers to mass uncertainty. Figures 5 and 6 illustrate the control laws and the corresponding system responses, respectively, in the case of a 20% increase over the vehicle's nominal body mass. On the other hand, the response of the two controlled systems and the control law in the case of 20% less than the vehicle's nominal body mass is depicted in figures 7 and 8, respectively. Tables 4 and 5 report the ISE's corresponding numerical value. As shown in figures 5 and 7, the control signals for both controllers remain within the actuator's permissible force limit for both cases. Furthermore, figures 6 and 8 demonstrate that the PD-NN exhibit a robust performance. In addition, the numerical validation of this result is provided in tables 4 and 5. Specifically, tables 4 and 5 demonstrate that varying the car body mass by ±20% does not affect the ISE index values for the PD-NN controller. However, compared to the results of the standalone PD, the PID, and the SF controllers, it can be observed that the PD-NN controller shows more robustness for both cases.

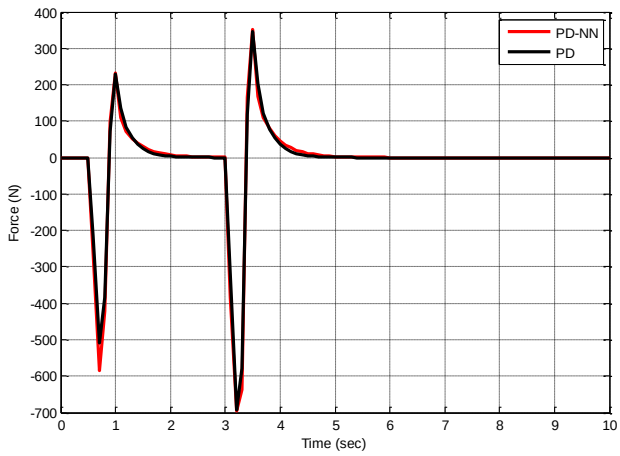

Figure 7. Control law of the controllers under a 20% decrease in the car body mass

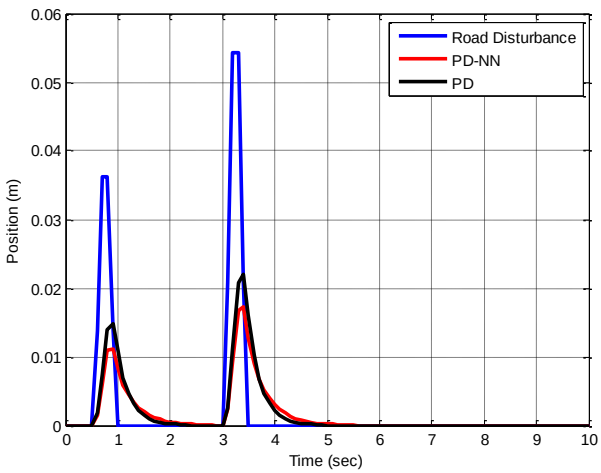

Figure 8. Suspension system response under a 20% decrease in the car body mass

Controller	ISE
PD-NN	1.5×10^{-3}
PD	2.2×10^{-3}
PID [24]	2×10^{-3}
SF [24]	2.4×10^{-3}

Table 4. Performance comparison under 20% decrease in the car body mass

6. Conclusion

Undesirable vibrations occur in suspension systems. In response to continuous changes in the business environment and market demand, an improved control system of the suspension system is an important contribution to riding comfort and the road-holding ability. In this paper, a PD-NN controller was successfully designed as an active controller for a nonlinear suspension system. The results showed that the proposed PD-NN controller is capable of satisfying all the pre-assigned design requirements within the actuator limitation. The NN was trained using the SLO technique based on minimizing the ISE index. The performance characteristics and the robustness of the proposed active suspension system were evaluated using computer simulation based on MATLAB. Moreover, the comparison results of the PD-NN controller with the standalone PD, PID, and SF controllers reveal that the PD-NN is more effective and robust in controlling the vehicle. This work can be extended in various directions as future work. For example, the present control algorithm can be applied to a full-car. In addition, to train the weights of the NN, other recent swarm optimization techniques can be used.

Authors'Declaration
The authors declare no conflicts of interest.

Authors' Contribution Statement
Huthaifa Al-Khazraji: Conceptualization, Methodology**,** Software**,** Writing-Original draft preparation, Writing-Reviewing and Editing
Mohanad Nawfal: Conceptualization, Methodology, writing-Original draft preparation
Russul A. Kadhim: Conceptualization, Methodology**,** writing-Original draft preparation
Mohammed M. Msallam: Conceptualization, Methodology**,** Software.
Omar F. Lutfy: Conceptualization, Methodology, Validation, Writing-Reviewing and Editing

References

1. M. Simion, L. Socaciu, and P. Unguresan, Energy Procedia **85** (2016) 472.
2. P. Danca, I. Nastase, F. Bode, C. Croitoru, A. Dogeanu, and A. Meslem, In IOP Conference Series: Materials Science and Engineering, Galati, Romania **595(**1) (2019) 012027.
3. L. Russi, P. Guidorzi, B. Pulvirenti, D. Aguiari, G. Pau, and G. Semprini, Sensors **22**(2) (2022) 543.
4. M. Lesage, D. Chalet, J. Migaud, and C. Krautner, Journal of Environmental Management **358** (2024) 120861.
5. L. Konieczny, P. Fabis, J. Matijošius, K. Duda, P. Deuszkiewicz, and A. Kilikevičius, Applied Sciences **15**(10) (2025) 5510.
6. N. Zhang, M. Fard, J. Xu, J.L. Davy and S.R. Robinson, Applied Ergonomics **114** (2024) 104148.
7. A.C. Mitra, G.J. Desai, S.R. Patwardhan, P.H. Shirke, W.M. Kurne, and N. Banerjee, Procedia Engineering **144** (2016) 1158.

8. M. Issa, and A. Samn, Mathematics and Computers in Simulation **191 (**2022) 328.
9. H. Al-Khazraji, Math. Model. Eng. Probl. **9**(2) (2022) 437.
10. A.M. Soliman, M.M. Kaldas, J. Low Freq. Noise Vib. Act. Control **40**(2) (2021) 1005.
11. M. Ghoniem, T. Awad, O. Mokhiamar, Alexandria Engineering Journal 59(5) (2020) 4013.
12. A. Hamza, N. Ben Yahia, Proc. Inst. Mech. Eng. Part I: J. Systems and Control Engineering 235(6) (2021) 952.
13. M. Yu, S.A. Evangelou, D. Dini, Engineering **33** (2024) 160.
14. M.A. AL-Ali, O.F. Lutfy, H. Al-Khazraj, Int. J. Intell. Eng. Syst. **17**(4) (2024) 870.
15. M. Gong, H. Chen, J. Low Freq. Noise Vib. Act. Control **39**(3) (2020) 787.
16. S. Rajala, T. Roinila, M. Vilkko, O. Ajala, J. Rauh, IFAC-PapersOnLine **50**(1) (2017) 14519.
17. G.W. Abedulabbas, F.R. Yaseen, Math. Model. Eng. Probl. **9**(6) (2022) 1523.
18. F.R. Al-Ani, O.F. Lutfy, and H. Al-Khazraji, Journal of Robotics and Control (JRC) **6**(1) (2025) 22.
19. V.I. Lachin, V.S. Elsukov, M.N. Mustafa, 2015 Int. Siberian Conf. Control and Communications (SIBCON) (2015) 1.
20. Y. Shahid, M. Wei, Algorithms **13**(1) (2019) 10.
21. C.P. Cheng, C.H. Chao, and T.H. Li, In 2010 IEEE International Conference on Systems, Man and Cybernetics (2010) 1939.
22. X. Dai, C. Zhao, R. Xu, 2023 3rd Int. Conf. Electronic Information Engineering and Computer Science (EIECS) (2023) 633.
23. J. Zhang, Y. Yang, C. Hu, Mathematics **11**(12) (2023) 2626.
24. M.A. Al-Ali, O.F. Lutfy, H. Al-Khazraj, J. Robot. Control **5**(4) (2024) 1041.
25. E. Kemer, H. Başak, Res. Eng. Struct. Mater. **11**(1) (2025) 45.
26. D. Koulocheris, G. Papaioannou, D. Christodoulou, Mobility Veh. Mech. **42**(2) (2016) 17.
27. E. Carpanzano, D. Knüttel, Appl. Sci. **12**(21) (2022) 10962.
28. M.M. Msallam, N. Alawad, A.K. Al Mhdawi, A. Al-Khazraji, S.S. Husain, and A.J. Huamidi, IET Conf. Proc. CP913 **2024**(37) (2024) 650.
29. K. Al-Badri, H. Dulaimi, H. Al-Khazraji, and A.J. Humaidi, Journal of Robotics and Control (JRC) **6**(2) (2025) 1061.
30. M.G.M. Abdolrasol, S.S. Hussain, T.S. Ustun, M.R. Sarker, M.A. Hannan, R. Mohamed, J.A. Ali, S. Mekhilef, A. Milad, Electronics (Basel) **10**(21) (2021) 2689.
31. O.F. Lutfy, A.L. Jassim, Eng. Technol. J. **36**(12 Part A) (2018) 1290.
32. H. Al-Khazraji, A.R. Nasser, S. Khlil, IAES Int. J. Artif. Intell. **11**(2) (2022) 649.
33. S. Khlil, H. Al-Khazraji, Z. Alabacy, IOP Conf. Ser.: Mater. Sci. Eng. **745**(1) (2020) 012175.
34. A. Dafid, A.I. Sudianto, R. Thinakaran, F. Umam, F. Adiputra, Izzuddin, R.S. DeboraJurnal Ilmiah Teknik Elektro Komputer dan Informatika (JITEKI) **11**(2) (2025) 238.
35. H. Al-Khazraji, S. Khlil, Z. Alabacy, J. Mech. Eng. Res. Dev. **43**(2) (2020) 74.
36. A.K. Ahmed, H. Al-Khazraji, S.M. Raafat, Int. J. Robot. Control Syst. **4**(1) (2024) 331.
37. R. Masadeh, B.A. Mahafzah, A. Sharieh, Int. J. Adv. Comput. Sci. Appl. **10**(5) (2019) 388.
38. H. Al-Khazraji, Int. J. Prod. Manag. Eng. **10**(1) (2022) 91.
39. B.M. Nguyen, T. Tran, T. Nguyen, G. Nguyen, Int. J. Comput. Intell. Syst. **15**(1) (2022) 90.
40. H. Al-Khazraji, K. Al-Badri, R. Almajeez, A.J. Humaidi, Int. J. Robot. Control Syst. **4**(4) (2024) 1547.